A Finite Element Method Based Approach for Evaluating the Sensitivity of Faraday-Type Electromagnetic Flow Meter for Liquid Sodium Flow

Udaya Kumar
Associate Professor, Department of Electrical Engineering
Indian Institute of Science, Bangalore
INDIA – 560 012
uday@hve.iisc.ernet.in

K.K. Rajan
Director, Fast Reactor Technology Group
IGCAR, Kalpakkam
INDIA – 603102
kkrajan@igcar.gov.in

Abstract—**Faraday-type electromagnetic flow meters are employed for measuring the flow rate of liquid sodium in fast breeder reactors. The calibration of such flow meters, owing to the required elaborative arrangements is rather difficult. On the other hand, theoretical approach requires solution of two coupled electromagnetic partial differential equation with profile of the flow and applied magnetic field as the inputs. This is also quite involved due to the 3D nature of the problem. Alternatively, Galerkin finite element method based numerical solution is suggested in the literature as an attractive option for the required calibration. Based on the same, a computer code in Matlab platform has been developed in this work with both 20 and 27 node brick elements. The boundary conditions are correctly defined and several intermediate validation exercises are carried out. Finally it is shown that the sensitivities predicted by the code for flow meters of four different dimensions agrees well with the results given by analytical expression, thereby providing strong validation. Sensitivity for higher flow rates, for which analytical approach does not exist, is shown to decrease with increase in flow velocity.**

Keywords- Flow meter, Faraday-type, Electromagnetic flow measurement, liquid sodium flow

I. INTRODUCTION

For various technical reasons, the liquid sodium is employed as a coolant [1] in both primary and secondary circuits of fast breeder reactors. For both monitoring and control, the flow rate of liquid sodium needs to be closely monitored [2 & 3]. Amongst flow meters of different kind, Faraday-type electromagnetic flow meters have been commonly employed [3]. Its principle and associated problems are described in [4].

In this type of flow meters, an external magnetic field is applied across non-magnetic steel pipe carrying liquid sodium. The direction of flow being orthogonal to the applied magnetic field generates electric field in the conducting liquid sodium. Due to the non-uniform flow across the cross section, the resulting induction will also be non-uniform. This induced field leads to circulating currents, which finds closed path majorly through the pipe wall. This in turn results in potential difference across different points on the wall cross section with maximum difference occurring across the bisecting diagonal plane orthogonal to the external applied field. This potential difference, in principle, is proportional to the average flow, provided the reaction field is not strong [4].

In Indira Gandhi Centre for Atomic Research (IGCAR) Faraday-type electromagnetic flow meters of various dimensions have been successfully developed and employed. Alnico permanent magnet assembly is employed for producing the magnetic field. A schematic of the flow meter is given in figure 1. Wires are welded on the pipe wall for the voltage measurement.

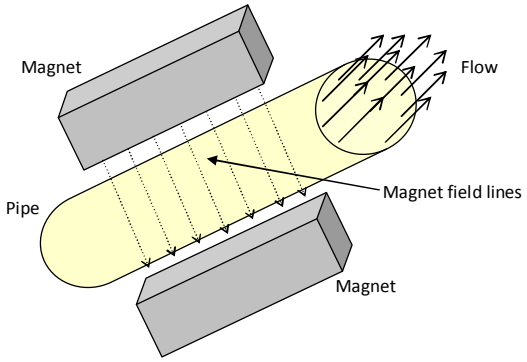

Fig. 1 Schematic of the flow meter

II. PRESENT WORK

The present work essentially employs the finite element approach presented in [3]. However, small correction on computational domain and boundary conditions were essential and they have been suitably incorporated. Typically in flow meter environment, the following assumptions are deemed to be valid. Firstly, the source of the external magnetic field is assumed to be unperturbed by the reaction field produced by the current induced in the liquid sodium. However, the resulting magnetic field will definitely be affected. Secondly,

the electromagnetic force on the liquid sodium is assumed to be insignificant as compared with hydraulic forces. Thirdly, the induction due to the turbulent component of the flow is shown to average out in time to zero [4].

Firstly, the governing equation will be deduced explicitly with nomenclatures employed in electrical engineering.

A. *Governing equations*

For a steadystate condition, the bulk current density satisfies

$$\nabla \cdot \vec{J} = 0 \qquad \text{....(1)}$$

where, the current density is constituted by induction due to fluid flow across the magnetic field, as well as, resulting conduction field. Also, the magnetic field is constituted by the external applied field ($\boldsymbol{B_a}$) and the induced reaction field ($\boldsymbol{B_r}$). Similarly, the electric field at any point can be written as [4]:

$$\vec{E} = -\nabla\emptyset - \vec{u} \times \left(\vec{B}_a + \vec{B}_r\right) \qquad \text{...(2)}$$

where $\boldsymbol{u}$ is the fluid velocity function. Combining above two, we get:

$$\nabla \cdot (\sigma \nabla\emptyset) + \nabla \cdot \left(\sigma \vec{u} \times \left(\vec{B}_a + \vec{B}_r\right)\right) = 0 \qquad \text{...(3)}$$

The above equation completely defines the conduction field. Now to define the magnetic field both divergence and curl of magnetic field is to be defined. The applied (external field) while ensuring the divergence property, yields null contribution to the curl in the analysis domain. Therefore, curl of the reaction field only arises, which is defined by the Amperes law in point form:

$$\nabla \times \left(\frac{1}{\mu_0} \vec{B}_r\right) = -\sigma\left(\nabla\emptyset + \vec{u} \times \left(\vec{B}_a + \vec{B}_r\right)\right) \qquad \text{...(4)}$$

Invoking the magnetic vector potential $\boldsymbol{A}$ for further processing, the above equation can be reduced under Coulomb's gauge as:

$$-\nabla\left(\frac{1}{\mu_0} \nabla \cdot \vec{A}\right) + \sigma\nabla\emptyset - \sigma \vec{u} \times \left(\nabla \times \vec{A}\right) = \sigma \vec{u} \times \vec{B}_a \qquad \text{...(5)}$$

It may be noted here that only the vector potential due to induced current is considered in the formulation. Similarly, equation 3 can be re-written as:

$$\nabla \cdot (\sigma \nabla\emptyset) + \nabla \cdot \left(\sigma \vec{u} \times \left(\nabla \times \vec{A}\right)\right) = \nabla \cdot \left(\sigma \vec{u} \times \vec{B}_a\right) \qquad \text{...(6)}$$

Equations 5 & 6 fully govern steadystate electromagnetic field in the flow meter. Next the finite element based numerical solution will be discussed.

B. *Galerkin formulation*

The Galerkin's Finite Element Method has been suggested and employed for the solution of the problem in [3]. Following the same, the weighted residuals of the equations 5 & 6 can be obtained as [3]:

$$\frac{1}{\mu_0}\int_V \nabla N \cdot \nabla A_i dV + \int_V \sigma N (\nabla\emptyset)_i dV - \int_V \sigma N [\vec{u} \times (\nabla \times A)]_i dV = \int_V \sigma N \left(\vec{u} \times \vec{B}_a\right)_i dV + \int_S N \frac{1}{\mu_0} \nabla A_i \cdot \vec{dS} \qquad \text{...(7)}$$

$$\int_V \sigma \nabla N \cdot \nabla\emptyset \, dV - \int_V \sigma \nabla N \cdot [\vec{u} \times (\nabla \times A)] \, dV = \int_V \sigma \nabla N \cdot (\vec{u} \times \vec{B}_a) \, dV - \int_S \sigma N [\vec{u} \times (\nabla \times \vec{A})] \cdot \vec{dS} - \int_S \sigma N [\vec{u} \times \vec{B}_a] \cdot \vec{dS} + \int_S \sigma N \nabla\emptyset \cdot \vec{dS} \qquad \text{...(8)}$$

The subscript i in equation 7 is for the three Cartesian components of the fields. The RHS essentially involves know quantities. The surface integrals of scalar and vector potentials are to be specified at the problem boundaries and get cancelled automatically at the material interface boundaries of the problem (i.e. interface between liquid sodium & steel pipe and steel pipe and air). For the problem in hand, last term in the equation 7 and last three terms in equation 8 can be ignored.

Implementation of equation 7 & 8 has been carried out with both 20 and 27 node cubic (brick) isoparametric elements with Serendipity type interpolation function. Extensive verification exercises were carried out at various stages, which included verification for steady conduction and induction without any reaction field. For the former, comparison with analytical solution was sought, while for the latter, a separate code based on discrete source modelling is developed. All the simulation exercises were carried out on Pentium dual core quad running at 2.27 GHz with 4 – 6 GB RAM. To accommodate the final matrix, it is explicitly built as a sparse matrix and Matlab's BICG routine is employed for efficient iterative solution.

C. *Results*

The finite element discretisation employed is shown in figure 2. Pipe axis is oriented along the Z-direction. Close to the pipe wall, the velocity profile show a sharp fall and hence refined meshing is adopted. As the surrounding medium is air, no current can leak through the pipe wall and hence homogeneous Neumann boundary is specified on pipe wall for the scalar potential. On the other hand, magnetic field can spread into the air and non-magnetic steel pipe cannot constraint it. Therefore the magnetic vector potential should not be set to zero, which was the mistake in [3]. In view of the same, the surrounding air medium is considered in the present work. At the same time, to limit the number of unknowns, suitable outer boundary needs to be defined and it is set at twice the pipe radius. This even though may not be an ideal choice can still aid in the solution as the current inside flows in opposite direction to that at pipe wall. The axial boundaries are selected such that the induction, as well as, drag on the current flow lines induced by the flow is negligible. For the

presentation, only the results with 27 node cubic element are considered.

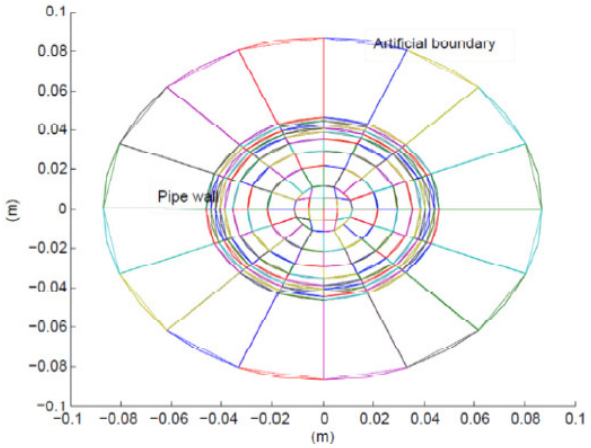

Fig. 2. Typical discretisation pattern

However in the simulation instead of actual velocity profile, an artificial velocity profile is employed with average velocity being held the same. This assumption on the velocity profile became necessary so as to restrict the number of elements and hence the number of unknowns (as demanded by the computer used). Sample velocity profile (called profile 1) across the radii of the pipe and axial variation in the applied magnetic field (which is x-directed) is given in figures 3(a) & 3(b) respectively. Sample simulation results for scalar electric potential and magnetic vector potentials are presented in figure 4. It may be noted here that additional routines were developed for the required contour and scatter plots. Figures 4(a) & (b) presents the equi-scalar potential surfaces traced in section planes. First figure is for a section plane bisecting the analysis domain across the pipe cross section, while the second figure corresponds to a section plane cutting pipe along the axis up to its center. It is clear from these figures that the induced current flows vertically up inside in the liquid metal and flows back along the pipe wall. As can be expected, the resulting potential will be highest at the middle of the domain.

The magnitude plot for the magnetic vector potential presented in figures 4(c) & (d), also describe the same pattern of current distribution. The magnetic field produced by the induced currents are presented in figures 4(e) & (f). The section planes are as in figure 4(a) & (b). This magnetic field circulates within the pipe both in upper and lowers half sections. At the entry side field is weakened, while it is strengthened at the exit side (refer to figure 4(f)). The role of this induced field becomes evident at higher flow velocities, which for smaller pipes typically exceeds the operating range dictated by other aspects.

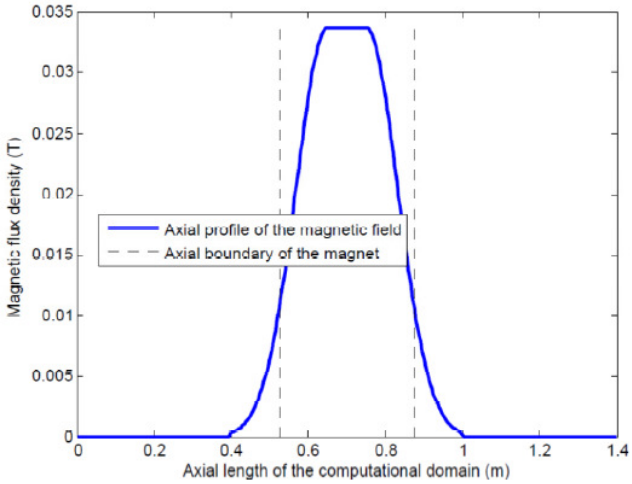

(a) Magnetic field

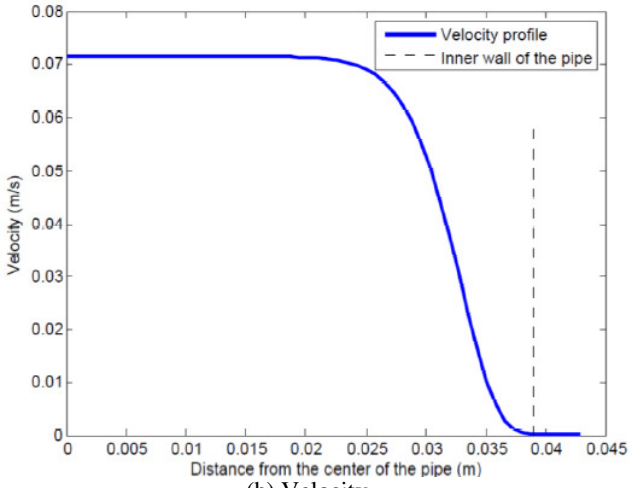

(b) Velocity

Fig. 3. Typical axial magnetic field and radial velocity profile1 employed in the analysis

Figure 5 presents the computed potential difference across the pipe section orthogonal to the applied magnetic field, where normally measurements are carried out. As can be expected, the potential difference assumes maximum at the middle of the analysis domain i.e. corresponding to middle of the magnet.

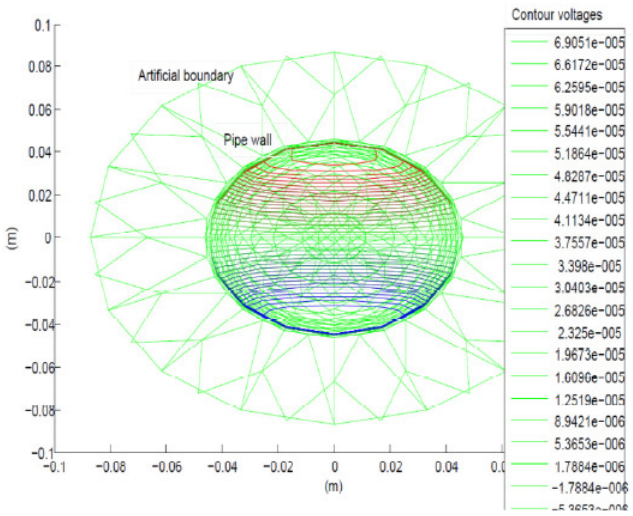

(a) Voltage distribution across c/s in the middle

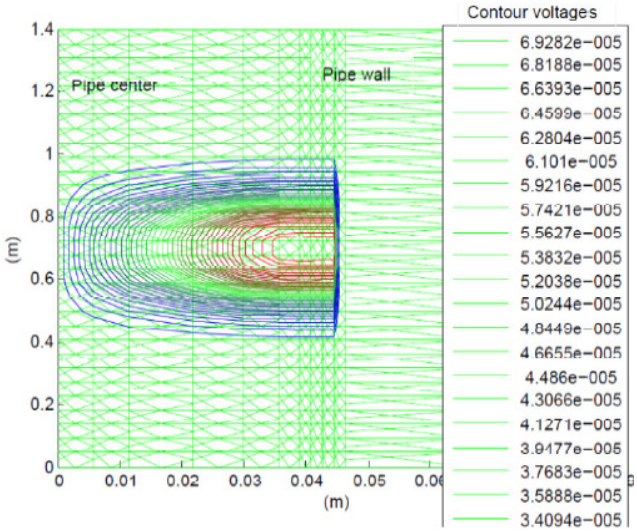

(b) Voltage distribution across c/s plane going up to the middle of the pipe

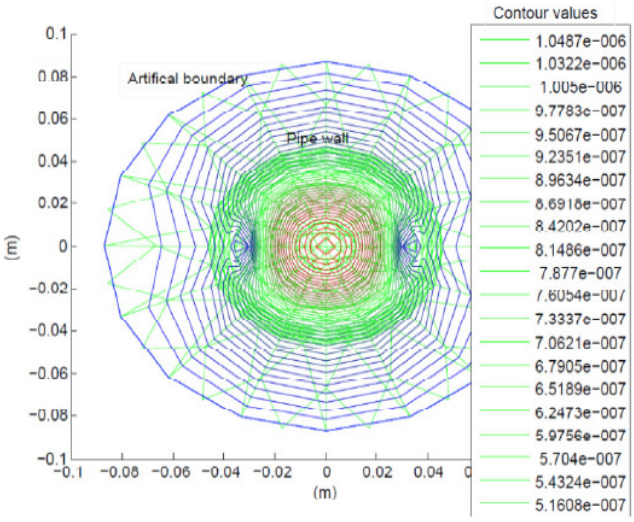

(c) Vector potential across c/s

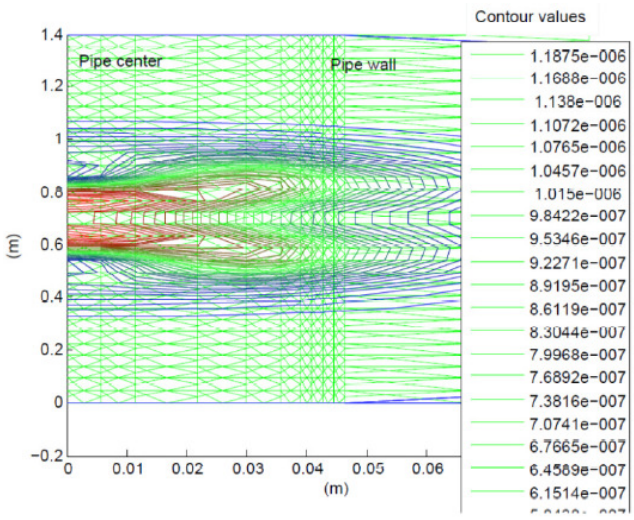

(d) Vector potential across bisecting plane going up to the middle of the pipe

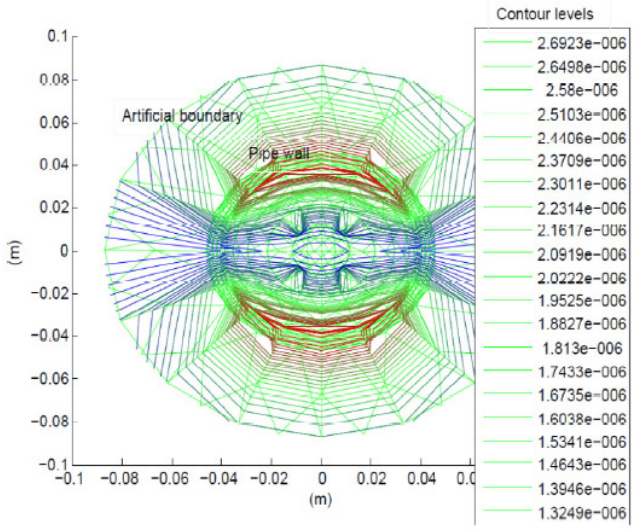

(e) Magnitude of the induced magnetic field across c/s at the middle

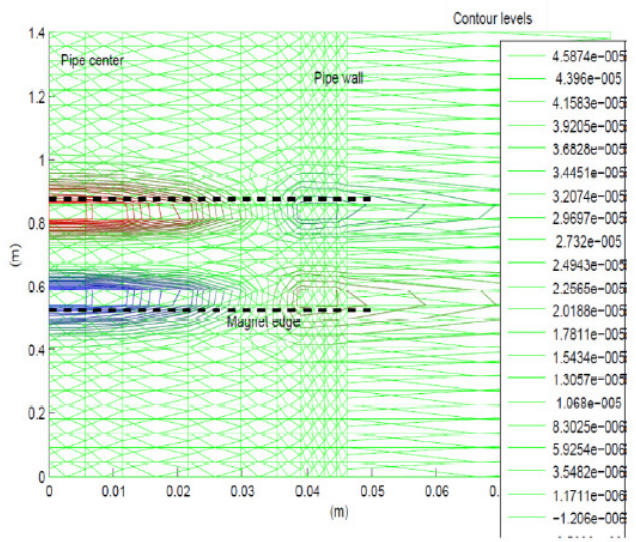

(f) Induced magnetic field across bisecting plane going up to the middle of the pipe

Fig. 4. Sample simulation results

Computations were carried out for flow meters of different dimensions. Table 1 presents the input data along with the analytical and computed sensitivities of the flow meter. It should be noted here that the analytical deduction is based on an axial-symmetric model for the problem, which could be employed for cases where the applied field is more or less constant for a length equal to pipe diameter, reaction field is rather weak, flow is laminar and measurements are made at the section plane bisecting the magnet. It will be evident from the table that FEM based evaluation of sensitivity is very accurate. The maximum difference between theoretically and analytically deduced sensitivities is within 4%, which can be attributed to several sources, including the assumed velocity and applied magnetic field profile.

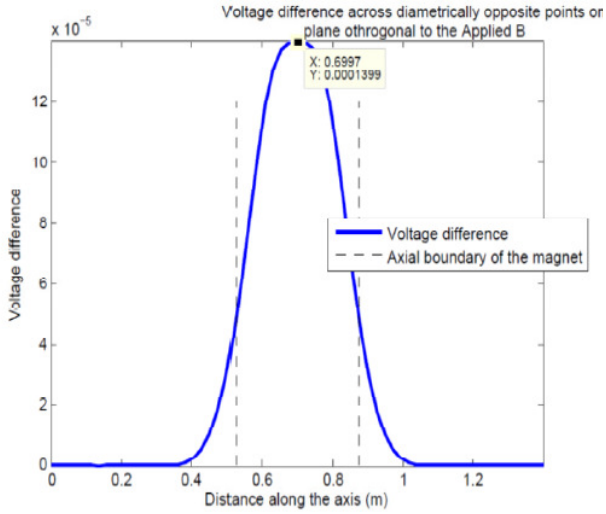

Fig. 5. Potential difference across points on pipe wall lying on the vertical bisecting plane

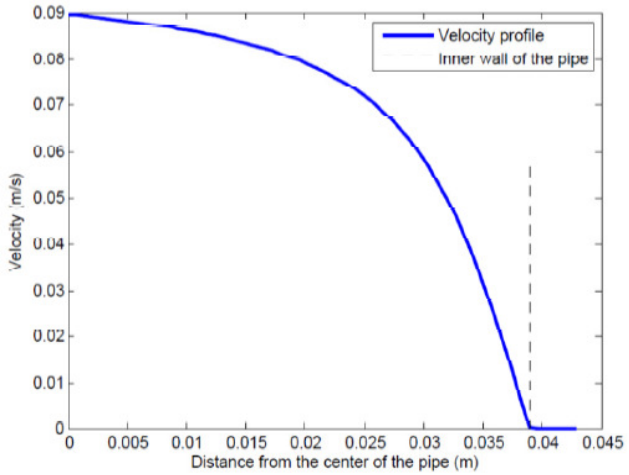

Fig. 6. Velocity profile 2

The flow employed in these exercises corresponds to magnetic Reynolds number lower than unity. In other words, the reaction field is not strong enough to perturb the applied field. This was also verified by doing analysis without considering the reaction field, which corresponds to another analysis option made available in the code. This option obviously required less memory and runs faster.

As assumed velocity profile, which is different than actual one is employed in the above exercises, it was necessary to check whether the results are sensitive to employed velocity profiles. For this, simulations (without considering the reaction field) were repeated with another profile (called profile2) which is closer to typical flow patterns across pipes. The same has been presented in Figure 6. The corresponding results are presented in Table 1. It is evident that computed potentials differences are not very sensitive to the actual profile, provided the average flow is maintained the same.

Table 1. Comparison of analytical and computed sensitivities

	200 NB	150 NB	100 NB DE	80 NB DE
ID/OD (mm)	219.1/202.7	168.3/154.1	114.3/102.3	88.9/77.92
Bstabilised (T)	0.02798	0.03366	0.03366	0.03366
Average velocity (m/s)	0.0086	0.01489	0.03379	0.05825
Sensitivity ** (mV/m^3/h) (analytical)	0.0447	0.0709	0.109	0.1418
Sensitivity (mV/m^3/h) (computed with profile 1)	0.04443	0.07133	0.1125	0.1476
Sensitivity (mV/m^3/h) (computed with profile 2)	0.04226	0.06788	0.1125	0.1475

** Actually equals to the induced voltage for the above velocity

As in all the above exercises, the relative strength of reaction field was rather insignificant, the associated validation remains inadequate. The actual strength of the code can be evident only at high magnetic Reynolds number for which the reaction field i.e. the magnetic field produced by the induced currents becomes comparable to the main applied field. However, the limited computer resources at present do not permit simulation for complete range of parameters. Hence, only limited simulation could be carried out and the corresponding will be presented here.

The flow velocity of liquid sodium is increased from a low value to about 25 m for 80 NB pipe. The velocity beyond about 8 m/s is not practical. However as the case with pipe of smaller diameter is considered (for meeting the permissible discretisation constraint in the existing computer), increasing in speed was the only choice for obtaining required magnetic Reynolds number. The discretisation was kept minimal and the same in whole of the exercise. The resulting number of elements was 4960 and the corresponding number of unknowns was 1,40,261. This problem could be accommodated with the 6GB Ram of the existing computer. As a result of coarse discretisation, some small spatial ripple could be seen in the computed potentials at velocities beyond 20 m. As before the potential differences were computed. However, to show the effect of reaction field, the computed potential differences were scaled by potential computed without considering the reaction field (which vary linearly with velocity). The results obtained are presented in figure 7, wherein to have some generality, instead of actual velocity, the x-axis is given in terms of magnetic Reynolds number R_m ($R_m = \mu\sigma U_z D_h$) where σ is the conductivity of the liquid sodium, U_z is the z-directed velocity and D_h is the hydraulic diameter of the pipe). The reduction in output voltage seems to be in good agreement with the data given [3], which actually correspond to a much larger diameter pipe.

Even though higher discretisation was essential for analysis on 200 NB pipe, an attempt was made evaluate the flow meter sensitivity with inadequate amount of discretisation. The number of elements employed was 8480 and the corresponding number of unknowns was 2,50,149. Memory management required extensive use of paging, which made the corresponding computation highly time consuming. Also, the use of lower discretisation resulted in spatial ripple in the computed potential differences even at a velocity of 3 m/s. Only with an intention of giving the trend, the output voltage of the flow meter for 200NB pipe case is also given in figure 7. Evidently, as before, the sensitivity decreases with flow rate.

Interestingly, it can be seen that for flow rates corresponding to magnetic Reynolds number lower than unity, output is undisturbed indicating weak reaction fields. On the other hand, for higher flow rates and hence magnetic Reynolds numbers, reaction field distorts the main field and hence causes reduction of the output voltage.

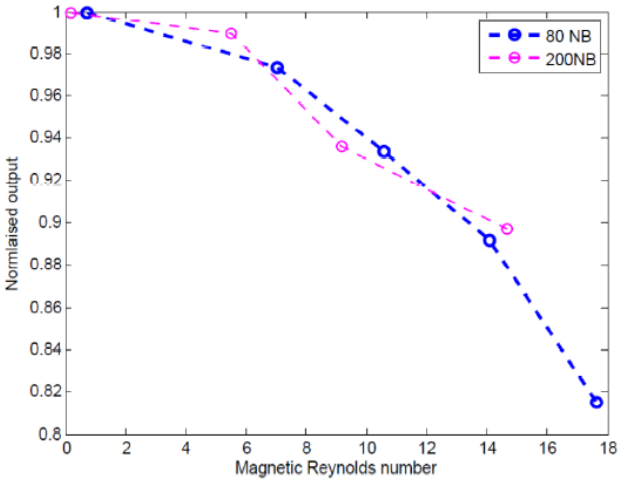

Fig. 7. Variation in normalised output with flow velocity

III. Summary and Conclusions

Faraday type Electromagnetic flow meters are widely employed in liquid metal fast breeder reactor for both monitoring and control. Calibration of the sensitivity of the flow meter is an involved issue due to several reasons. Suitable theoretical approach is always preferable and the present work has dealt with the same.

A 3D finite element method based code has been developed in Matlab for ascertaining the sensitivity of the flow meter. Suitable discretisation scheme has been adopted along with appropriate boundary conditions. Both 20 and 27 node brick element option is provided in the formulation. For a specified magnetic field and flow velocity profile, solution for the electromagnetic field is sought through A-φ formulation. The code developed has been verified to be stable for desired range of flow velocities, provided adequate discretisation is employed.

The results obtained for lower flow rates exhibit very good matching with the value predicted by analytical expression thereby validating the code. At higher flow rates, there is reduction in sensitivity caused by reaction field. The corresponding computed results exhibit a trend which is in good agreement with that given in the literature for a larger pipe.

The codes developed will be useful in flow meter calibrations and in future designs. It can also be employed for ascertaining the role of turbulence on measurements.

REFERENCES

[1] R.D. Kale and M. Rajan, "Developments in Sodium Technology", Current Science, Vol. 86, No. 5, March 2004.

[2] Summary of meeting, "Proceedings of the Specialist Meeting on Sodium Flow Measurements in Large LMFBR Pipes", Bergisch Gladbach, Germany, 4-6th February 1980.

[3] Takahiro M. and Hideo A., "Characteristic evaluation of electromagnetic flow couplers using a liquid metal MHD analysis code", Nuclear Engineering and Design 235 (2005) 1503–1515.

[4] Shercliff, J.A., "The theory of electromagnetic flow measurement", the University press, Cambridge, UK, 1962.